CONE-AXIS DIFFRACTION PATTERNS

D. Jerome Fisher, *University of Chicago, Chicago 37, Illinois*

Abstract

Cone-axis x-ray pictures have been described briefly by Buerger (1944). They are obtained when a lattice translation direction is given a precessing motion with respect to the direct beam, providing a flat film is placed in the holder of the precession camera which is normally occupied with the layer-line screen. The result is a series of diffracted spots which lie along concentric circles ("rings"), one for each level of the reciprocal lattice within range. A cone-axis photo bears about the same relation to a precession picture that a rotation film has to a Weissenberg.

While cone-axis photos are useful in determining the value of d^* in the direction of the precessing crystal axis, they have a number of other possible uses, as herein discussed. After a short introduction to the precession technique, the present paper outlines the methods for indexing the spots on these pictures. A number of features of cone-axis films are then discussed under miscellaneous remarks, after which the use of these patterns for orientation purposes is briefly described. The paper concludes with a section on the Laue streaks found on these films.

Introduction to the Precession Technique

The Buerger precession camera (here assumed to be set up for a fixed, collimated horizontal x-ray beam) consists basically of a bed carrying a pair of two-axis universal joints whose centers are offset by a distance F along a horizontal line which coincides with the undiffracted beam.[1] Each joint comprises a horizontal and a vertical axis, like an oarlock; oscillation about these is so coupled that the resultant movement of a chosen direction (a crystal axis) through the center of the joint is that of the generatrix of a cone whose axis is the undiffracted beam. In the same way when the handle of an oar on a rowboat is moved along a circular path, the oar itself (like the crystal axis) becomes the generatrix of a cone. Figure 13[2] shows a simple model which illustrates this condition. One end of the rod representing the precessing crystal axis is pointed; this fits in a groove in the end of a cylinder (whose axis coincides with the direct beam) so that this pointed tip may be moved about a circular path. The two wire grids represent fantastically-enlarged levels of the reciprocal lattice (as cut off by the sphere of reflection) normal to the precessing axis. On the precession camera the two universal joints are tied together through a parallel linkage in such fashion that they partake of identical motions.

[1] A photograph of the current model of this instrument (as made by Charles Supper) appears as Fig. 6 on p. 100 (Fisher, 1952 *b*). V_{x1} is the vertical axis through the crystal and V_{ca} is the one through the film cassette.

[2] The numbers here assigned to figures, tables and formulas are in continuation of those used for the same purposes in earlier papers (Fisher, 1952 *b*, *c*).

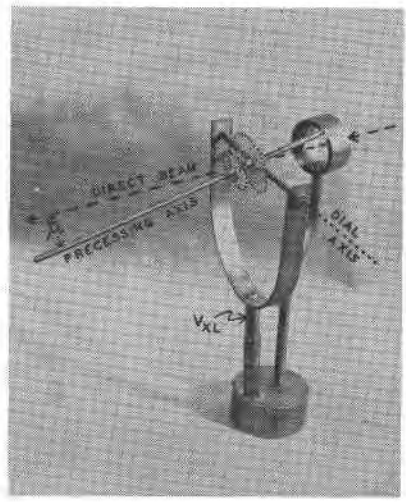

FIG. 13. Model to illustrate the first universal joint of the precession set-up. V_{x1} is the vertical axis through the crystal; the latter is also on the horizontal dial axis.

The crystal is mounted at the center of the first joint (at S, Fig. 14) so that its horizontal oscillation axis, called the dial axis, is parallel to a reciprocal axis (or any desired translation direction of the reciprocal lattice) of the crystal. The dial axis moves in a horizontal plane (as it oscillates back and forth on the vertical axis of the joint); the dial axis is thus normal to the direct beam at only two moments during a single

»»→

FIG. 14. Vertical cross-section of the precession set-up (includes the direct beam and the $\bar{\mu}$-arc). This is a scale drawing to fit the sphalerite photo of Fig. 17, except that $s'=30.22$ mm.

Symbols

D—Distance, crystal to 0-level film measured normal to the film (SP_0).

F—Distance, crystal S to center Z_0 of 0-level film along the path of the undiffracted beam.

$\bar{\mu}$ (bar mu)—Angle between the direct beam and the normal to the reciprocal lattice levels (the precessing crystal axis).

$\bar{\nu}$ (bar nu)—Half apical angle of an n-level diffraction cone.

0—Points on the one-level film: 0_c=center; 0_0=0-level diffraction cone; 0_1=1-level diffraction cone.

P—Points on the precessing crystal axis: P_r=sphere of reflection; P_c=cone axis film; P_1=1-level film; P_0=0-level film.

R—Points in the reciprocal lattice: R_0=0-level (zero-point at R_0); R_1=1-level.

S—Center of crystal, at center of the sphere of reflection.

Z—Points on the zero-level film: Z_0=0-level diffraction cone (film center at Z_0); Z_1=1-level diffraction cone.

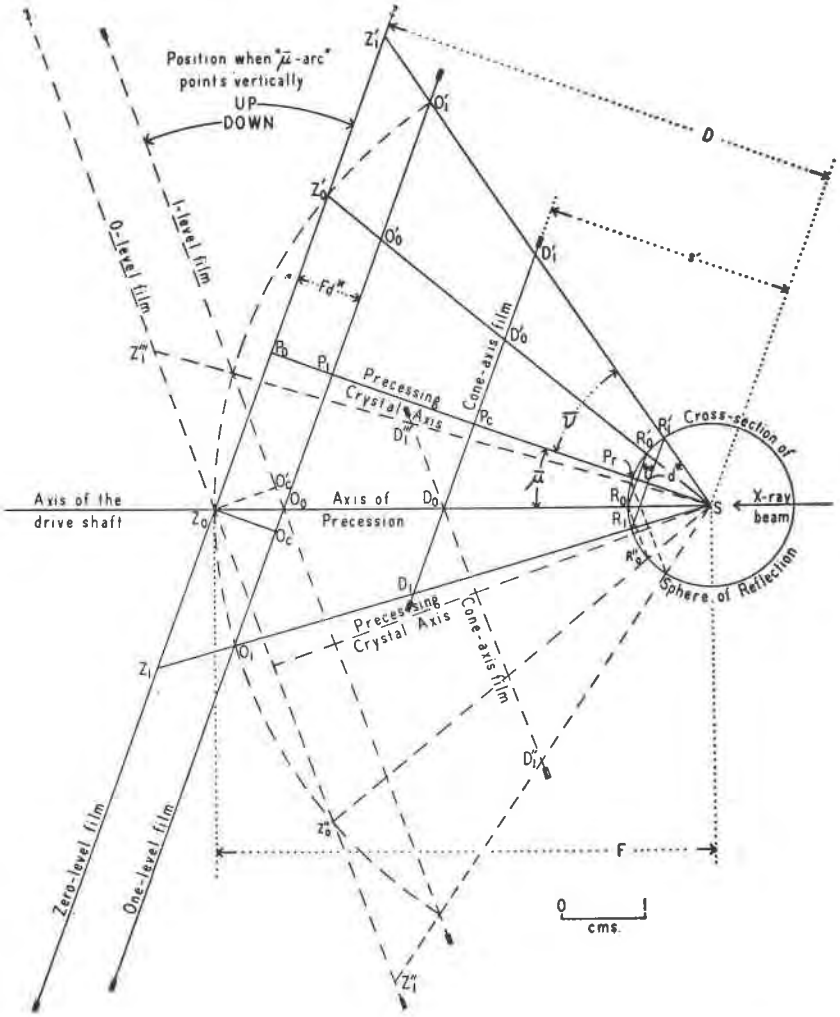

360° precession; these are the two positions of Fig. 14 (one shown by solid lines, the other with dashed lines); here the dial axis is normal to the paper through S. Mounted on the dial axis (and so partaking of a precessing motion identical with that of the crystal) is a bracket carrying the layer-line screen holder in which may be placed a plane layer-line screen (having an annular opening) at a distance s from the crystal, or a cone-axis flat-film cassette, with distance s' from crystal to film (measured normal to the screen holder). The layer-line screen is used when taking ordinary precession pictures, so that diffracted beams from but a single level of the reciprocal lattice can strike the film.

The plane film for taking a precession picture, which is an undistorted enlargement of a limited portion of some one level of the reciprocal lattice, is mounted in a cassette suspended in the second universal joint, whose center coincides with Z_0 (at a distance F from S, Fig. 14), the center of the zero-level film which lies on the undiffracted beam. For taking n-level precession pictures the cassette is moved towards the crystal a distance Fd^* along an axis normal to the film; n-level film is thus always parallel to that of the 0-level, but is closer to the crystal by a variable distance Fd,* where d^* is the spacing (measured in reciprocal lattice units) between adjacent levels of the reciprocal lattice measured along the precessing axis. The center of an n-level film is at O_c, which does not lie on the undiffracted beam during precession.

Since the crystal is mounted on the dial axis with a reciprocal lattice translation direction parallel this axis, levels of the direct lattice must lie normal to it. Thus the dial axis may be clamped at an azimuth position read on the dial such that a crystal axis (or some chosen translation direction of the direct lattice) lies in a horizontal plane (when the precessing position is 90° off that shown diagrammatically in Fig. 14)[3] and is normal to the dial axis. Under these conditions the crystal axis is set to undergo a precessing motion. The instrument is so designed that the angle (designated $\bar{\mu}$; read "bar mu") between the precessing crystal axis and the finely-collimated x-ray beam may be varied from 0° to about 30°; in Fig. 14, the value is 20°, one in common use. This setting is made by moving the "film-normal shaft" along the "$\bar{\mu}$ arc" attached to the front end of the horizontal drive shaft (the axis of which coincides with the undiffracted beam); the solid line part of Fig. 14 represents the condition where the $\bar{\mu}$ arc is up, and the dashed line part fits when this arc is down. The film-normal shaft is parallel to the precessing crystal axis, thus it is always normal to the dial axis, the $\bar{\mu}$-arc, and the film. When $\bar{\mu}=0°$, no precession occurs and so the crystal axis is parallel to the x-ray beam. Moreover with this angle set to 0° the instrument is suitable for taking flat film transmission Laue photos.

It is obvious that levels of the reciprocal lattice (R_0, R_1, etc. of Fig. 14) must lie normal to the precessing direction, since the latter is a crystal axis. These levels being planes cut the sphere of reflection in concentric circles whose common center is P_r (the point where the precessing crystal axis pierces the sphere of reflection). Thus the diffracted beams that "flash" out momentarily from any one level of the reciprocal lattice as the crystal undergoes its precessing motion must lie along a conical

[3] Actually the crystal is mounted when the $\bar{\mu}$-arc is set to 0°. Thus the chosen crystal axis is made horizontal (by adjusting the azimuth reading on the dial) without respect to any particular precessing position.

surface, the *diffraction* cone, whose axis is the precessing crystal axis, and whose half opening angle is designated $\bar{\nu}$ (read "bar nu"). Since the cone-axis film partakes of the same precessing motion as the crystal, and one identical with it (not offset from it, as is true for the various level precession films), the cones of diffraction for the various levels cut this film in a series of concentric circles or "rings." The diameters of these appear in Fig. 14 as D_0D_0' for the 0-level, D_1D_1' for the 1-level, etc.[4] A cone-axis picture is reproduced in Fig. 17*b*. Note from Fig. 14 that one generatrix for the 0-level diffraction cone (that from S to D_0) coincides with the undiffracted x-ray beam. Thus

$$r_0 = s' \tan \bar{\mu} \tag{39}$$

where r_0 is the radius of the 0-level cone-axis ring. Since the instrument is set to a given $\bar{\mu}$ value, and r_0 can be measured from the film, this equation is convenient for computing s', the distance from the crystal to the film. Knowing this value and measuring r_1 (the radius of the 1-level cone-axis ring on the film) enables one to compute $\bar{\nu}_1$ (the half-apical angle for the 1-level diffraction cone), since

$$r_1 = s' \tan \bar{\nu}_1. \tag{40}$$

It will be noted that $\bar{\nu}_0 = \bar{\mu}$. Thus the latter symbol is employed for this angle, so that in general $\bar{\nu}$ can be used without a subscript when one is discussing some particular n-level. Of course if d^* is known, $\bar{\nu}$ can be computed from

$$\cos \bar{\nu}_n = \cos \bar{\mu} - d^* \tag{41} \text{ [Buerger, 1944 (14)]}.$$

In making precession photos of the various levels, since the film cassette precesses off the universal joint centered at Z_0, offset by a distance F from the crystal, the diffraction cone from any one level shears over the film about a circular path, in contrast to the situation for the cone-axis film. Thus for cone-axis pictures the points D_1 and D_1' in one position of Fig. 14 go to the points D_1'' and D_1''' respectively in the other position; it will be noted that D_1 and D_1'' are the same distance from the bottom edge of the film. In similar fashion corresponding points Z_1 and Z_1' on the zero-level film in the "$\bar{\mu}$ arc up" position go to points Z_1'' and Z_1''' respectively in the other position, but it is clear that while Z_1 is only a short distance below the center of the film, Z_1'' is near the bottom edge. In short as the diffraction cone precesses, a larger *precession cone* is generated; the axis of this coincides with the undiffracted beam, and its half opening angle is $\bar{\mu}+\bar{\nu}$.

[4] In using Fig. 14 one should always remember that the sphere of reflection shown on it is purely schematic, and not drawn to the scale given. Thus its radius is unity; this may be thought of as 1 A (where λ is measured in A). Thus SZ_0 ($=F$, which is generally 6 cms.) is 600,000,000 times as great as SR_0!

Indexing Cone-Axis Pictures

In indexing a cone-axis film it is first desirable that each level on it be converted to the same scale as the level precession film. Since each level of a series of precession pictures is photographed at a different distance from film to crystal (so that the resultant films can be superposed, with the reciprocal lattice grid developed on the same scale on each one), whereas the several levels appear on a single cone-axis film, it is clear that each cone-axis ring must be enlarged by a different factor to fit the proper level precession film. Of course this enlargement can be avoided by taking a series of cone-axis films at different s' values, one to fit each distance value of the various level precession films; but this technique is too time-consuming as well as expensive to be practicable.

While the scale of each level precession film may be reduced to fit that of the proper cone-axis ring, the reverse procedure is generally simpler, since it merely involves moving each spot on a given ring out radially a suitable distance. This is conveniently done by making a trace-o-film[5] copy of the spots of any ring, drawing radii through these, and adding another set of spots where these radii cut a newly-drawn circle of suitable radius r_D.

Taking first the n-level case, specifically the 1-level of Fig. 14, it is clear that the normal distance D from the crystal to the 0-level film is $F \cos \bar{\mu}$, and to the 1-level film is $D\text{-}Fd^*$. Thus from similar triangles the radius r_D of the 1-level cone-axis ring enlarged to the scale necessary to fit the 1-level precession pattern is given by (42), where r_D' is the radius of the 1-level ring measured on the cone axis film.

$$r_D = [r'_D(D - Fd^*)]/s'. \tag{42}$$

In Fig. 15 is given a copy of the 1-level precession photo of a sphalerite. Four circles are added to this as follows:

- P, the outcrop of the precession cone of radius r_P.
- D, the outcrop of the diffraction cone (its radius is r_D) at a given moment (when the center of its ring is at c_D).
- B, the area of no spots or blind area with radius r_B.
- G, the guide circle of radius r_G. While precession occurs, the precessing crystal axis (axis of the diffraction cone) moves along G.

It is obvious from the dotted line $tc_D = r_D$ of Fig. 15 that

$$r_G = r_D - r_B. \tag{43}$$

Referring to Fig. 14, it is clear that a circle with center S and radius F will intersect SZ_1 at O_1, since it is simply an F enlargement of the trace

[5] This is a .003″ thick colorless transparent cellulose acetate sheet with matte finish on one side obtainable in convenient rolls from The Lustro Co., 2455 S. Archer Ave., Chicago 16, Ill.

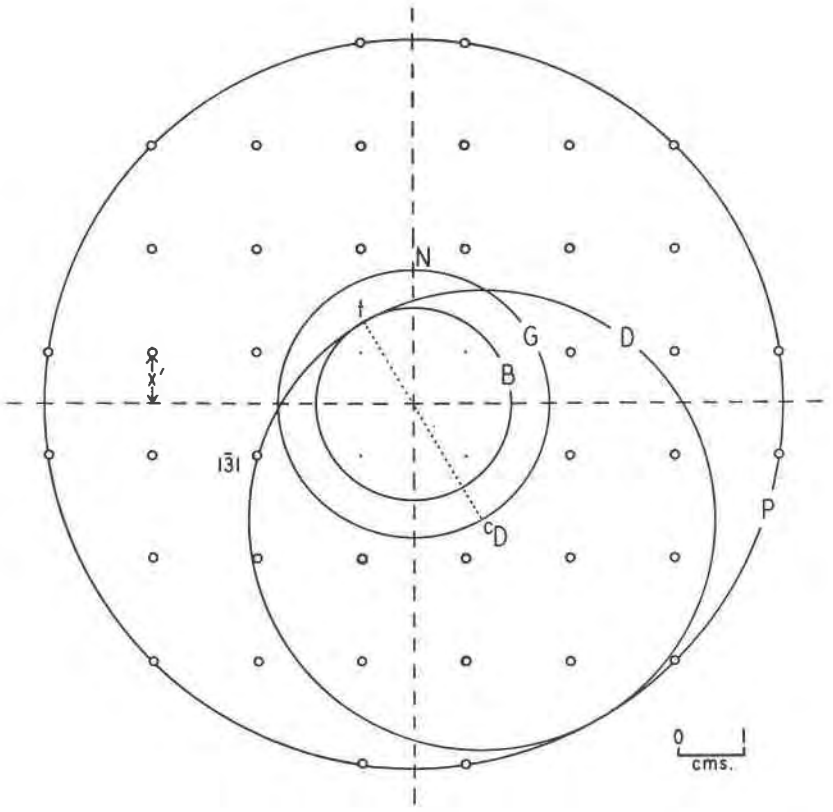

FIG. 15. Copy of 1-level precession photo along [a] of sphalerite ($a_0=5.401$; with $x'=0.7895$ cms. for MoK$_\alpha$ radiation where $F=6.000$ cms.; $\bar{\mu}=20°$).

of the sphere of reflection. Thus $SO_1=F$ and sin $\bar{\nu}=P_1O_1/F$. But $r_B=O_cO_1=P_1O_1-P_1O_c$, and $P_1O_c=P_0Z_0$ (since Z_0O_c is parallel to the precessing crystal axis) $=F$ sin $\bar{\mu}$. Thus

$$r_B = F(\sin \bar{\nu} - \sin \bar{\mu}). \tag{44}$$

Thus using the results of (42) and (44) to compute (43), one is able to draw the guide circle on the precession film or a copy traced from it (Fig. 15). If desired, the precession circle P may also be drawn, since $r_P=r_D+r_G$.[6]

[6] Circles B and P often show up as the mid-circles of shaded annular areas on n-level precession films. These areas mark where most of the scattered general radiation getting through the annular slot of the layer line screen strikes the film. The center for the circles bounding these shaded areas generally fails to coincide with the center of the film simply because the center of the layer line screen cannot be lined up exactly.

As precession is taking place, the circle D shears around so that it remains tangent to the outside of B and the inside of P, while its center c_D keeps on G. Under these conditions when D intersects a spot of the precession photo, such a point represents the location of a diffracted spot on the cone-axis ring D of the same index as the spot on the precession film; this is illustrated for $(1\bar{3}1)$ for the particular position of D given in Fig. 15. Assuming that one is looking in the direction of travel of the x-rays, if the drive shaft of the precession instrument rotates clockwise, then c_D (which represents the outcrop of the precessing crystal axis) moves about G in clockwise fashion also; in Fig. 15 a position of D is shown when c_D has moved 150° along G from the "north" position N (that represented by the solid lines of Fig. 14). It is instructive to think of Fig. 15 while watching a precession picture "in the making"; then c_D

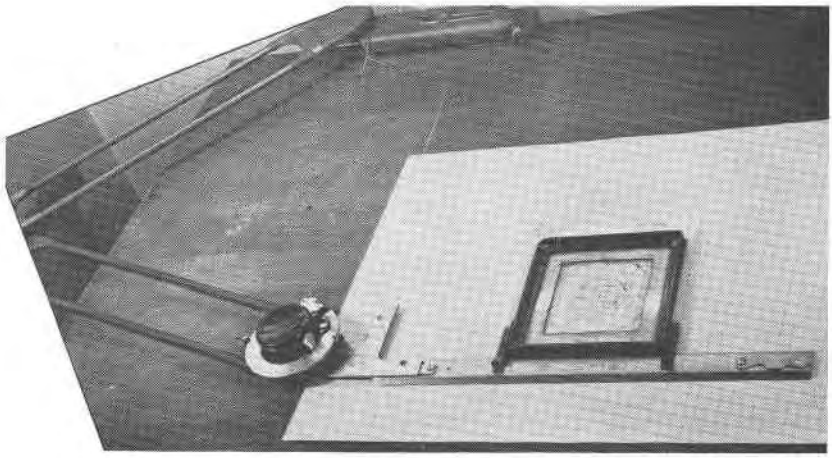

FIG. 16. Set-up for indexing the spots on a trace-o-film enlargement of a cone-axis ring.

corresponds to the center of the layer-line screen (the point where the precessing crystal axis intersects the screen), and the "central circle" of the annular opening is represented by D.

All the spots on the trace-o-film enlargement of the 1-level cone-axis ring can be indexed quickly if it is mounted with Scotch tape on a simple hollow rectangular framework which is temporarily attached to one arm of a universal drafting machine as shown in Fig. 16. The latter is set so that the cardinal directions of the cone-axis ring enlargement always stay parallel the cardinal directions of the 1-level precession photo (or tracing thereof, which is attached to the drawing board) while c_D on the enlargement is moved about circle G drawn on the precession picture.

The 0-level case may be handled by using a simplification of (42) in which Fd^* is omitted, but it is easier to use

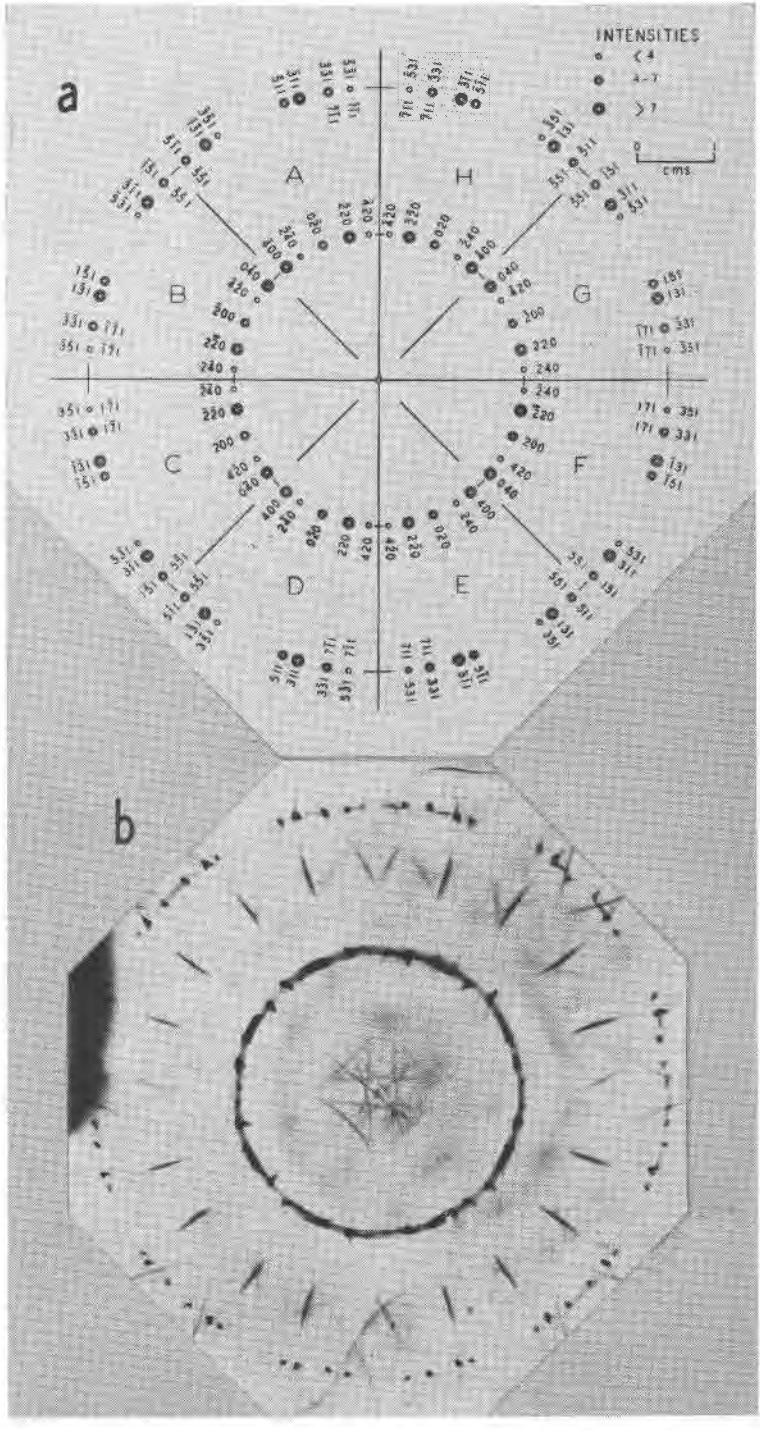

FIG. 17. Cone-axis picture of sphalerite with precession on [*a*] and dial axis [*a*.]
(*a*) Diagram to show spot-indices for 0- and 1-rings.
(*b*) The actual photo. MoK$_\alpha$ radiation, $\bar{\mu}=20°$, $s'=51.4$ mm.

$$r_D = F \sin \bar{\mu} \tag{45}$$

which is obvious from Fig. 14. Since for the 0-level $\bar{\nu}=\bar{\mu}$, equation (44) shows that $r_B=0$, and thus it follows from (43) that $r_D=r_G$.

Figure 17*a* is a copy of a cone-axis film of sphalerite with the spots for the 0- and 1-level rings indexed. A replica of the actual photograph appears as Fig. 17*b*.

An excellent exercise for students trying to visualize the precession technique consists in reversing the procedure just described. That is, the tracing of the spots of the 1-level precession photo is correctly mounted in the framework on the arm of the universal drafting machine and moved about over the proper enlargement of the 1-level cone-axis ring attached to the drawing board, so that some point of circle *G* drawn on the tracing of the precession photo is always above c_D, the center of

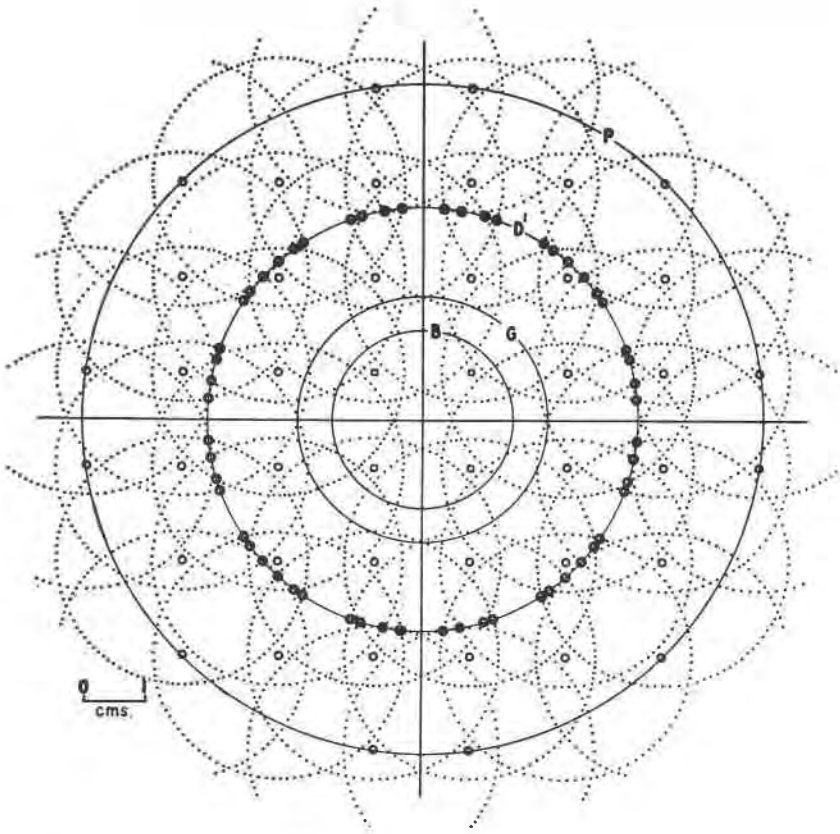

FIG. 18. Diagram to illustrate the method for indexing the spots of the 1-level cone-axis ring of sphalerite.

the cone-axis ring. Of course this is the same as saying that the center of the precession film should be moved about the circumference of a circle G drawn on the cone-axis enlargement. This gives the illusion that the 1-level grid of the reciprocal lattice is precessing through the base D of the calotte cut out of the enlarged sphere of reflection by the plane of the grid. Under these conditions whenever a point on the grid reaches circle D, this corresponds to a reciprocal lattice point cutting the sphere of reflection, and so angular and spacing relations are correct for diffraction to occur. This technique is not handy for actual indexing, since the sheet to be indexed is covered by the one having the spots of known index.

The procedure just described can be restated as follows. If the suitably enlarged 1-level cone axis ring D' is drawn with its center at the center of the 1-level precession grid (see Fig. 18), and if each point of this grid is made the center of a circle of radius r_G, then these circles (dotted in Fig. 18) will cut the circle D' at points marking diffracted spots on the enlarged cone-axis ring D'. This is illustrated in Figs. 18 and 19 for the 1- and 0-levels respectively of sphalerite, where the dotted circles have radius r_G with centers at the points of the level precession grid. In the absence of a universal drafting machine, this method will be of value.

In case of a non-orthogonal relationship between the various levels of the reciprocal lattice normal to the precessing crystal axis, the procedures just described need be modified only to allow for the shear between the grids of the various levels; for all levels the B, G, D', and P circles are centered at the (000)* point. This is illustrated by Fig. 20*a* for chalcanthite[7] (Fisher, 1952*b*) with [*b*] as the precessing axis, and $F=6.00$ cms. for the 1-level. This diagram shows enough of the reciprocal net grids for the 0- and 1-levels so that they can be completed if desired; also the B, G, and P circles can be added from the data given. It is clear that the 0-level grid is on a smaller scale than that of the 1-level; both grids are drawn proper scale to fit the respective cone-axis rings. Figure 20*b* is a reproduction of the actual cone-axis film, which also shows much of the 2-level ring; the light area along the upper left side marks where the film was shielded by a portion of the goniometer head; the light annulus about the 0-level ring is due to the direct beam-stopping cup, and the two light streaks extending to the right (and sloping down) from this are due

[7] In Fig. 20*a* the spots on the 1-level ring are indexed as if they belonged to the $\bar{1}$-level. This is necessary in non-orthogonal situations if the 1-level reciprocal lattice grid is to correspond to the gnomonogram of morphology (Fisher, 1952*a*). This apparent anomaly arises since in precession work levels are taken as positive when going from near the surface of the sphere of reflection (the 0-level) towards the center, whereas in morphology the 0-level cuts the center of the unit sphere and the 1-level is near its surface.

to the arm supporting this cup. The spots on the 0-level ring are not very clearly discernible on the print because of the heavy general radiation reflection trail (Laue streak) that coincides with this ring; these spots are easily seen on the original film. Some of the elliptical Laue streaks associated with the 1-level shown in Fig. 20*b* are reproduced in Fig. 20*a;* these are discussed later.

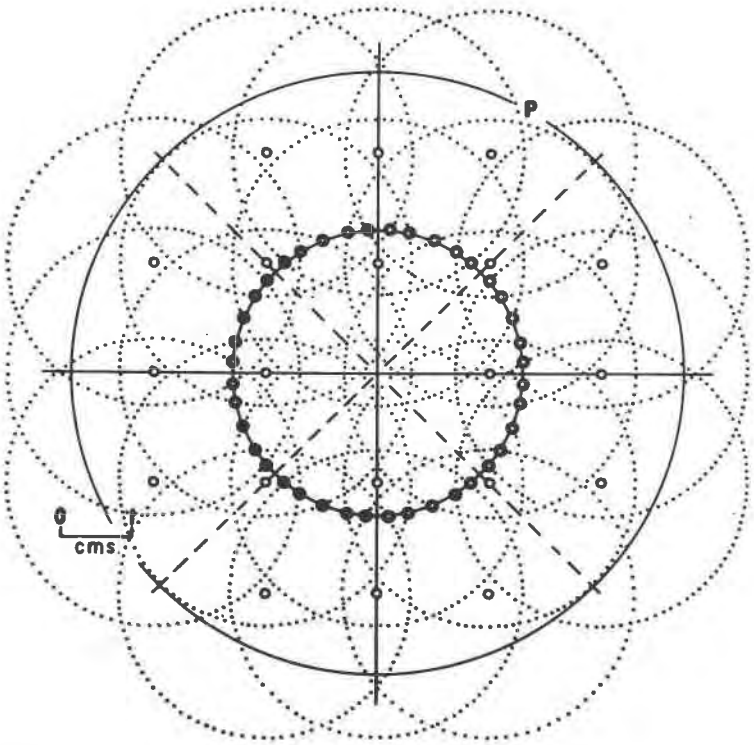

FIG. 19. Diagram to illustrate the method for indexing the spots of the 0-level cone-axis ring of sphalerite.

MISCELLANEOUS REMARKS

It will be noted that in general each spot on a given precession film is represented by two on the corresponding cone-axis ring. Diametrically-opposite spots on the 0-ring (which are present in all cases) have the same indices, but with all signs changed. The condition in this respect for the *n*-rings depends on the symmetry of the crystal. Thus the 0-ring condition is duplicated on the *n*-rings for sphalerite[8] (Fig. 17), but in

[8] Of course in the case of opposite spots on *n*-rings there is no change in sign for the index digit which corresponds to the precessing crystal axis.

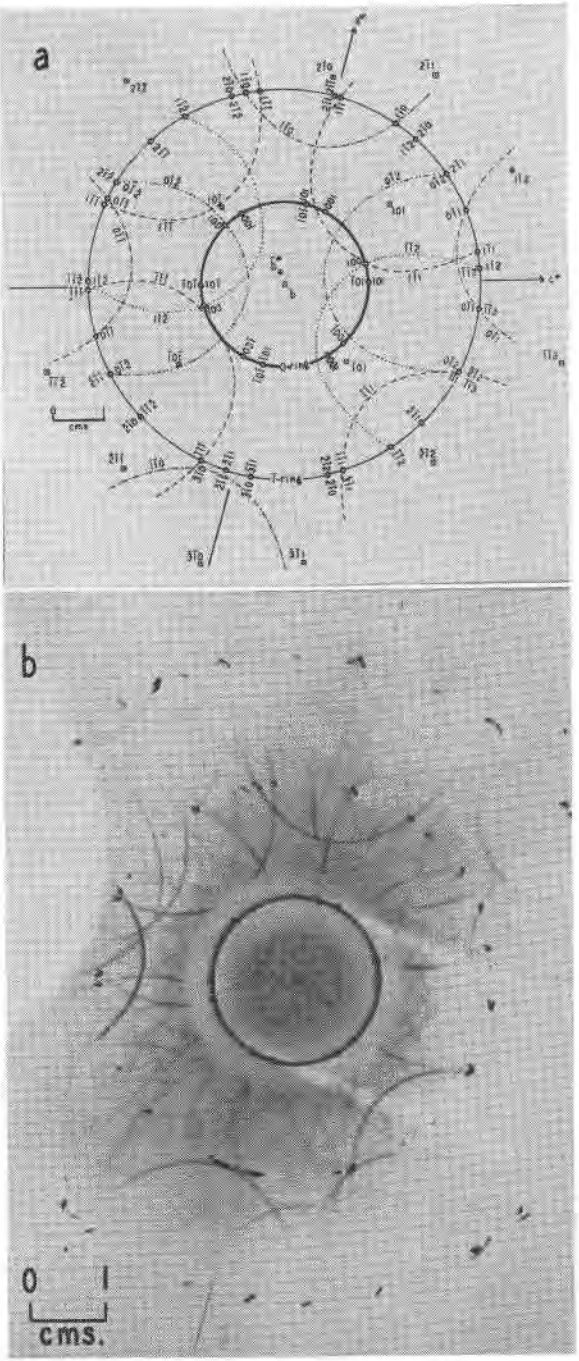

FIG. 20. Cone-axis picture of chalcanthite with precession on [b] and dial axis [c^*]. (a) Diagram to show spot indices for 0- and $\bar{1}$-rings; also some of the Laue streaks through the spots on the $\bar{1}$-ring. (b) The actual photo (with some of the 0-ring spots touched up a bit). FeK$_\alpha$ radiation, $\bar{\mu}=20°$, $s'=30.5$ mm.

the case of chalcanthite (Fig. 20) the n-rings are not marked by diametrically opposite spots. This presence or absence of symmetry is also well shown by the n-level Laue streaks. This is particularly noticeable for the (110) streaks in Fig. 20; the one near the top cuts the $\bar{1}$-ring in pronounced fashion, whereas the one near the base barely misses it. Buerger (1944, p. 9) has called attention to the advantages of the use of cone-axis patterns (as compared to Laue photos) for the determination of diffraction symmetry.

Those interested in quantitative intensity studies from precession films might find it advantageous to use cone-axis photos. Each spot on a level precession negative is a composite made by two beams diffracted at different moments during a single 360° precession. Such a composite spot appears as two separate ones on a cone-axis ring; these two should be of equal intensity. If spots along any given ring are too thickly spaced for satisfactory intensity measurements, this situation can be remedied by any or all of the following three techniques: (1) decrease the $\bar{\mu}$-angle; (2) increase the wave-length of the x-rays; (3) increase the distance s' from crystal to film.

While the 0-ring is of no value in determining d^*, certain features of it are of interest. The radius of this ring depends solely on $\bar{\mu}$ and s', and is independent of λ. Thus a single 0-ring is obtained for both K_α and K_β radiation (this, of course, is not true for n-rings). Moreover, the 0-ring may be used to derive the geometrical constants of the crystal, just as is true for the 0-level precession film. This is illustrated in Fig. 21. It will be noted here that straight lines through the two (002)* spots and the two $(00\bar{2})^*$ spots, and lines through the two (200)* spots and the two $(\bar{2}00)^*$ spots, yield a network whose sides are $\perp c^*$ and $\perp a^*$ respectively. If parallel lines are run through (000)*, a mesh at angle β^* is developed whose line "spacings" (see Fisher, 1952*b*, p. 100, footnote) are $t^*_{c^*}$ and $t^*_{a^*}$ respectively. From these values one can calculate a^* and c^* by using the following formulae:

$$a^* = t^*_{a^*}/(F\lambda) \quad \text{and} \quad c^* = t^*_{c^*}/(F\lambda). \tag{46}$$

Of course if γ and a are known, a and c may also be computed.[9] Note that the diagonal bisectors [through (000)*] of this mesh yield reciprocal translation directions (in the case of Fig. 21) of $[101]^*$ and $[10\bar{1}]^*$.

It is a simple matter to compute the angle A (measured along the 0-ring) between a spot on this ring and the point where it is cut by a reciprocal translation direction on which the spot would lie on a 0-level precession photograph. Such a translation direction is the perpendicular bisector of a line joining two spots of the same indices on this ring. Thus

[9] Using (54′) and (56′) of Fisher, 1952*c*, p. 698.

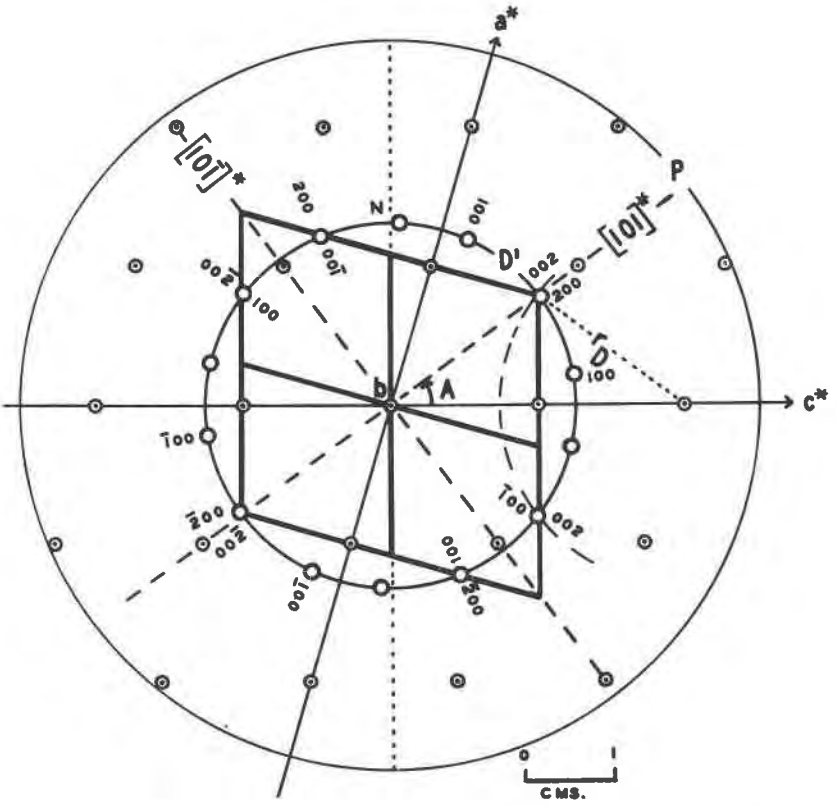

FIG. 21. Copy of an enlargement of the 0-ring of chalcanthite (same data as Fig. 20, except CuK_α radiation) to fit the $F=6.00$ cms. 0-level precession photo, copy of which is also shown.

for the two (002)* spots (where c^* is the given reciprocal translation direction):

$$\cos A_{(002)^*} = [(l/2)\cdot t^*_{c^*}]/r_D \tag{47}$$

in which l is the value of l in the index $(00l)^*$, and $r_D = F \sin \bar{\mu}$. The two (002)* spots are thus an angle A of 37°17′ measured along the 0-ring off the point where it is cut by c^*. The corresponding angle for one of the (200)* spots is 35°50′; thus these two spots are practically superposed.

In similar fashion one can compute angle A for all the "pinacoidal" spots on the 0-level ring. These may be combined as in Table 9 in a form that gives an interesting picture of how diffraction occurs on the precession instrument for the case of Fig. 21. As one looks in the direction of travel of the direct x-ray beam, counting azimuth angles clockwise (taking 0° when the $\bar{\mu}$-arc is vertically up) diffraction occurs for each

spot (also listing CuK_β reflections which are not shown in Fig. 21) when the $\bar{\mu}$-arc is in the azimuth position noted. Thus (considering only K_α spots) when the $\bar{\mu}$-arc has moved clockwise 23°56′ from its up (north) position, the center point c_D of diffraction ring D (see Fig. 15) lies above the (001) point on the D' ring in the upper right quadrant of Fig. 21, and the other (001) point (*lower* right quadrant of Fig. 21) marks where the diffracted beam then strikes the film. All the other diffracted spots are formed in similar more or less complementary order from that in

TABLE 9. AZIMUTH ANGLES FOR 0-LEVEL CONE-AXIS DIFFRACTION (ANGLES MEASURED CLOCKWISE FROM N TO FIT CONDITIONS AS GIVEN FOR FIG. 21)

Angle	Spot		Angle	Spot		Angle	Spot		Angle	Spot	
	K_α	K_β		K_α	K_β		K_α	K_β		K_α	K_β
21-03		001	126-57		$\bar{1}00$	201-03		$00\bar{1}$	306-57		100
23-26	001		127-17	002		203-26	$00\bar{1}$		307-17	$00\bar{2}$	
45-55		002	129-18	$\bar{1}00$		225-55		$00\bar{2}$	309-18	100	
52-43	002		134-05		002	232-43	$00\bar{2}$		314-05		$00\bar{2}$
54-10	200		151-26		$\bar{2}00$	234-10	$\bar{2}00$		331-26		200
60-48		200	156-34	001		240-48		$\bar{2}00$	336-34	$00\bar{1}$	
82-56	100		158-04	$\bar{2}00$		262-56	$\bar{1}00$		338-04	200	
85-17		100	158-57		001	265-17		$\bar{1}00$	338-57		$00\bar{1}$

which they are met in going clockwise around the D' ring. Thus the next spot formed is the (002)* in the *lower* right quadrant (made when the $\bar{\mu}$-arc reaches an angle of 52°43′ off N); the third spot is the (200)* of the upper left quadrant; the last (sixteenth) spot is the (200)* of the upper right quadrant. The position of the $\bar{\mu}$-arc for other (non-"pinacoidal") spots could be computed in a like manner. In short a 0-level general radiation reflection streak (ring) is "painted" one spot at a time, more or less as each "ring" on a "powder" film is really composed of many spots representing directions along which diffraction occurred from a given set of planes $n(hkl)$ in all possible orientations at a constant glancing angle θ.

The position of the "pinacoidal" spots of the 0-level cone-axis ring in terms of the angle A is shown by the graph of Fig. 22. This gives all such spots for precession on [b] (upper curve, right ordinate scale) as in Fig. 21 (if rotated 180° on the dial axis), and also for precession on [a] (lower curve, left ordinate scale). The spots actually located in Fig. 22 fit CuK_α radiation. Thus the (001) spot with A of 66°34′ is shown in Table 9 at a complementary value, and the (100) spot with A of 66°49′ in Fig. 22 appears in Table 9 at an angle of this value plus ($90°-\beta^*$). The positions

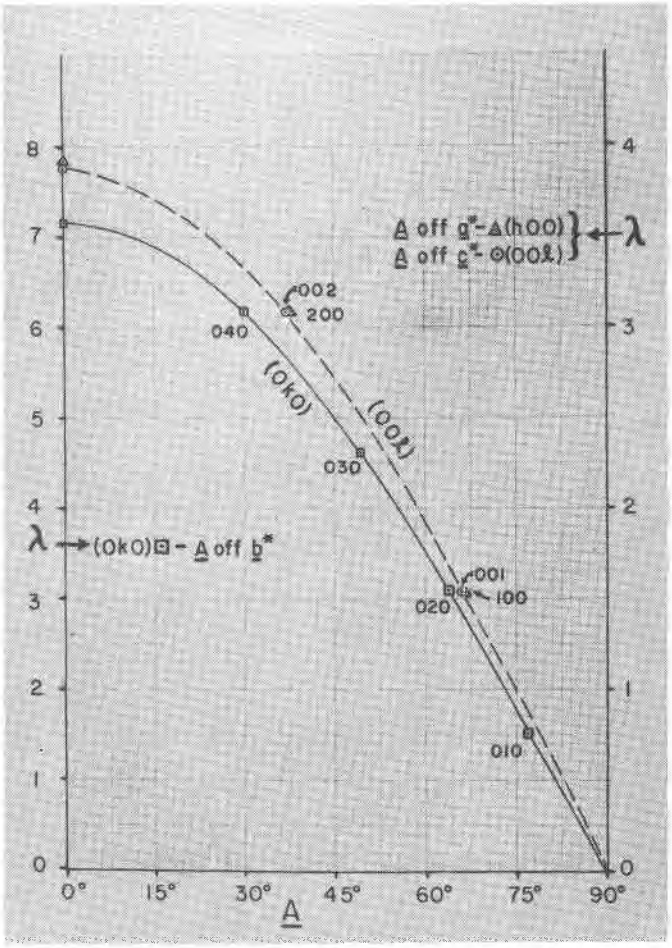

FIG. 22. Graph to show angle A for any "pinacoidal" spot of the 0-level cone-axis ring of chalcanthite for any possible radiation at $\bar{\mu}$ of 20° where the dial axis is [c^*].

of pinacoidal spots for radiation of any wave length can be read from Fig. 22 in similar manner. It can also be seen (left ends of curves) that the "unit pinacoid" spots of the 0-level ring would lie exactly on a reciprocal axis in the following cases:

(100) on a^* for $\lambda = 3.916$
(010) on b^* for $\lambda = 7.140$
(001) on c^* for $\lambda = 3.876$

These values are computed from equations (63), (59) and (65) of Fisher (1952*d*).

Knowing the positions of indexed spots for a 0-level ring also allows one to prepare a special layer-line screen useful in putting just a few calibration spots on any 0-level precession photograph. The writer has made such a screen for use with quartz ($\bar{\mu}=30°$; MoK_α radiation) precessing on [a^*] with [c] as the dial axis. This was finished by drilling small holes in a blank screen on a circle of $r=20$ mm. at angles A (measured off

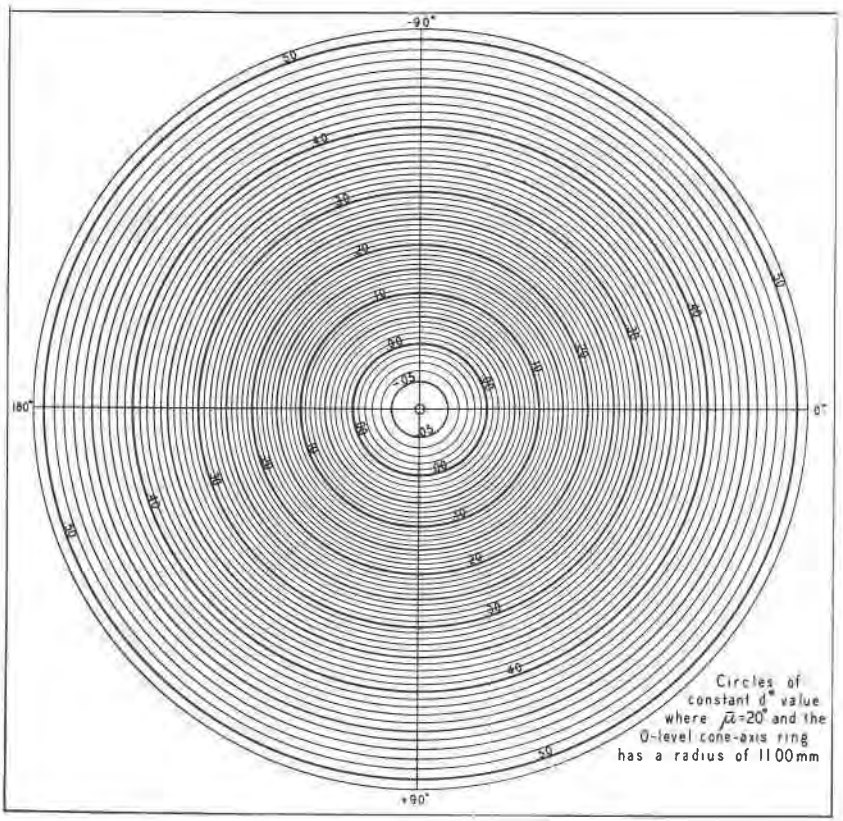

FIG. 23. Nomogram to furnish d^*-values from cone-axis photos where $\bar{\mu}=20°$; see text.

the dial axis) as follows: 2.°2 and 32.°5 for the (17) spots, and 60.°1 for the (30) spots. The center of the screen was found by letting the direct beam strike a small piece of fluorescent material fastened to it. In this way by keeping a quartz crystal accurately set on a goniometer head reserved for this purpose, one can make a double exposure on any 0-level precession photograph and thus have the quartz spots appear on it for purposes of calibration; by this scheme a large number of spots which

might cause confusion is avoided. Of course a similar screen could be made for use with a definite type of Laue photo from a given crystal.

The writer finds it convenient to take cone-axis photos at a distance s' of 30.22 mm. and $\bar{\mu}=20°$. Under these conditions no matter what the radiation the 0-ring has $r=11.00$ mm. If a glass positive is made from Fig. 23 so that the 0-ring has a radius of just 11.00 mm., then such a cone-axis film may be centered over the positive and the required spacing d^* (in reciprocal lattice units) for any n-level ring may be read directly from the graph.

Orientation from Cone-Axis Pictures

Cone-axis photos are normally not used for orientation with the precession camera, since it is ordinarily much more rapid to effect this by a technique described by Buerger (1944, 21–27) which employs unfiltered radiation and a small angle of precession. Under these conditions orientation can usually be reached quickly by adjusting the crystal until the Laue streaks (on the 0-level precession photograph made without a layer-line screen) radiating from the central spot are of equal lengths (see Fisher 1952*d*). However, the writer has been unable to employ this orientation technique in certain sulpho-salt work, whereas the cone-axis method yielded usable results.

When a translation direction of the direct lattice coincides with the precessing direction, a cone-axis photo may be obtained which yields diffraction spots along thin rings, one for each accessible level, if filtered radiation is employed. When the lattice translation direction deviates by a small angle from the precessing direction, the rings widen out into annular bands. Figure 24 shows a series of cone-axis photos of chalcanthite to illustrate this condition.

Figure 25 is a vertical cross-section through the cone-axis set-up to fit the case of Fig. 24*c* where the [*b*] axis of chalcanthite is off the precessing direction by 2° around the dial axis. In Fig. 25 the dashed lines represent the positions of the various reciprocal lattice levels drawn as they would be for perfect orientation; they are thus normal to the precessing direction and parallel the cone-axis film. The solid lines show the actual orientation of the levels normal to the [*b*]-axis; these are arranged in sheets, the thickness of each sheet corresponding to the shifting of that level due to the fact that it is not quite normal to the precessing direction. Thus when the $\bar{\mu}$-arc points vertically up, the 0-level lies along D_0K, the inner line (the one closer to the center of the crystal) of the 0-sheet; when it points vertically down, the 0-level lies along D_0K', the outer line of the 0-sheet. In between these two positions the 0-level lies at all possible intermediate (but parallel) positions. Thus as the precessing motion

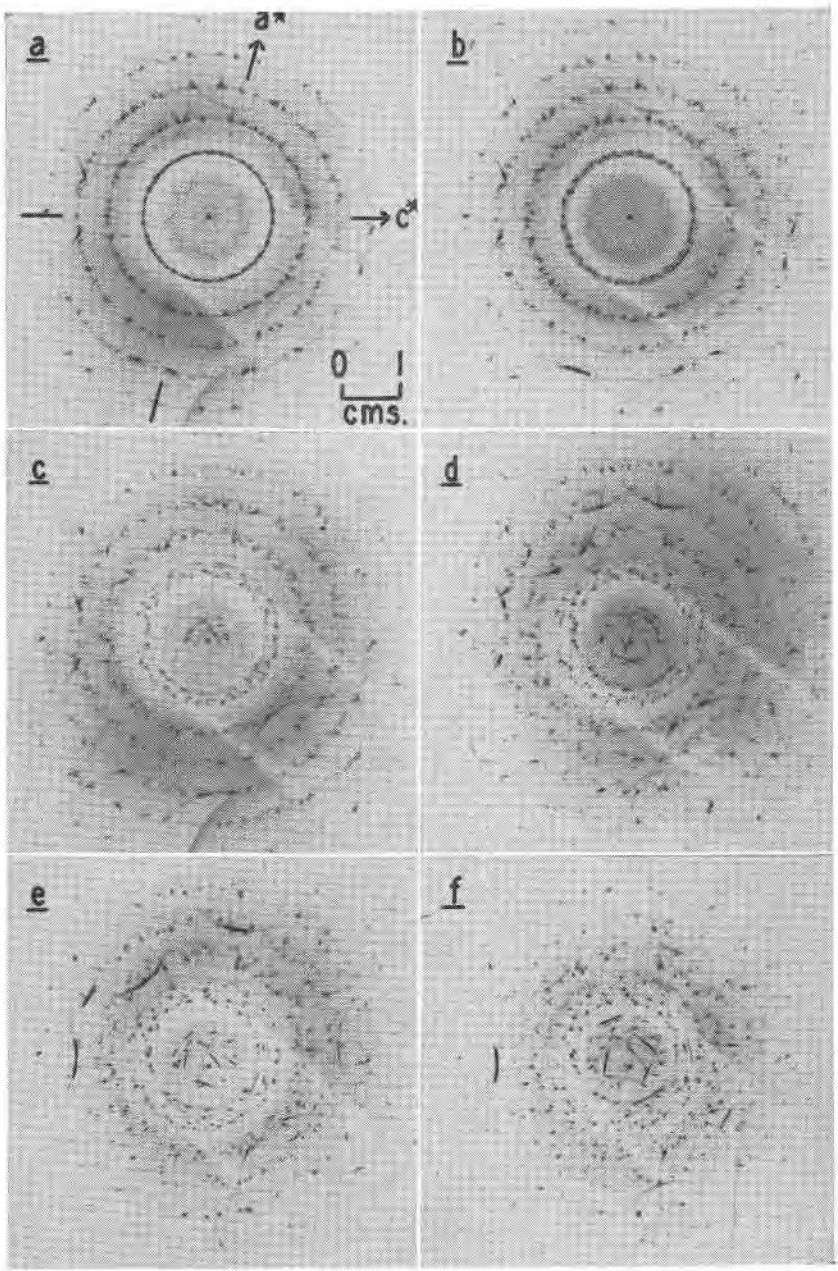

FIG. 24. Cone axis photos of chalcanthite. MoK$_\alpha$ radiation, $\bar{\mu}=20°$, $s'=30.22$ mm., [c^*] horizontal. Precessing direction is: (*a*) [*b*]; (*b*) 1/2° off [*b*] along dial (D) axis (parallel to [c^*]); (*c*) 2° off [*b*] along *D*; (*d*) 3° off [*b*] along *D*; (*e*) 3° off [*b*] along *D* and 1° off on vertical (*V*) axis; (*f*) 4° off [*b*] along *D* and 1° off on *V*.

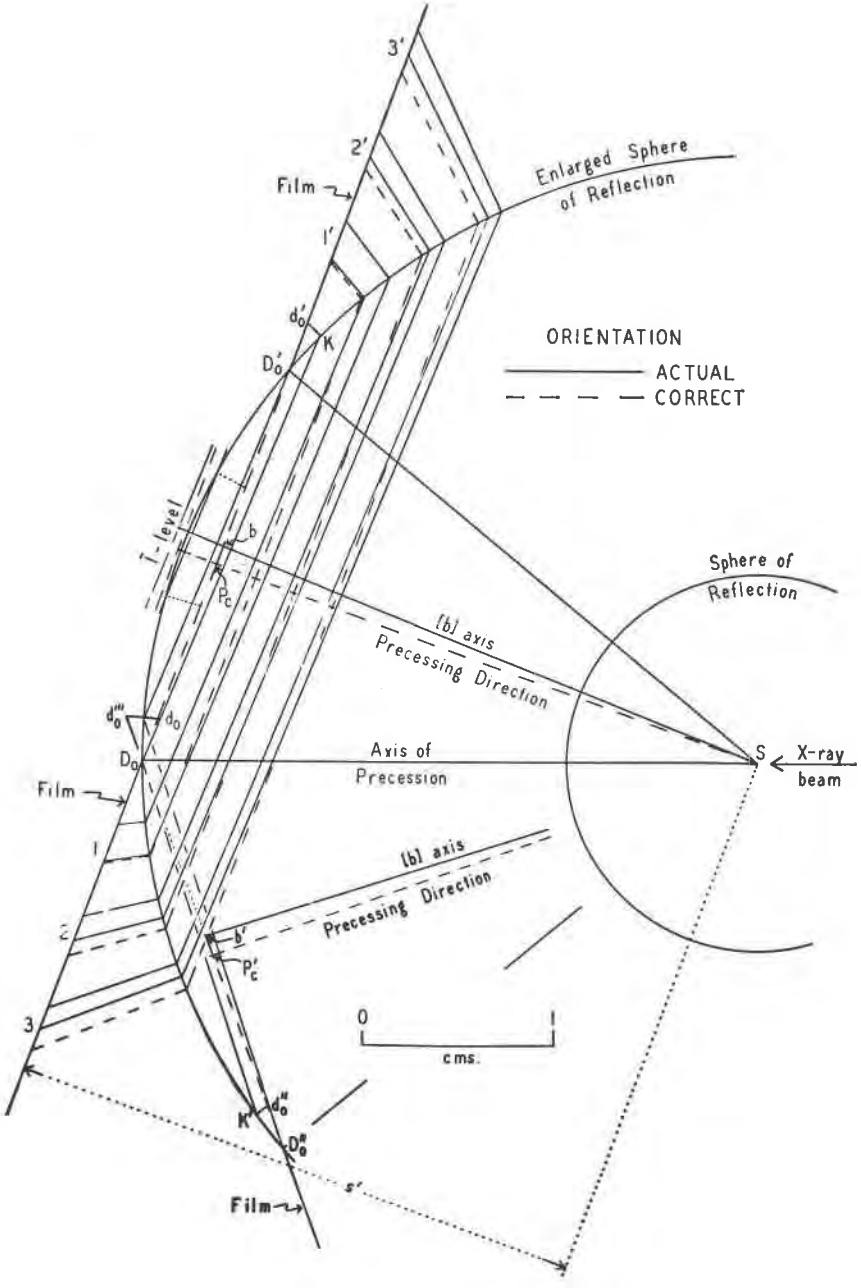

FIG. 25. Vertical cross-section through the cone-axis set-up to fit the case of Fig. 24*c*.

proceeds the 0-level moves in and out, sweeping over a spherical annulus of the enlarged sphere of reflection.

Thus the 0-level of the properly oriented crystal would give a sharp ring of spots on the film cutting through D_0 and D_0'. For convenience the enlarged sphere of reflection is drawn through these points. On the crystal oriented as shown in Fig. 25 with the $\bar{\mu}$-arc vertically up the 0-level ring forms an annulus of spots on the film through D_0d_0 and $D_0'd_0'$. This annulus is composed of spots which lie on near-circular ellipses; that is, the central projection of the various 0-level diffraction cones (whose axes coincide with [b], and not with the precessing direction) yields a series of near-circular ellipses on the flat film (which is normal to the precessing direction). After 180° precession, so that the $\bar{\mu}$-arc points vertically down, the annulus of spots goes through D_0d_0''' and $D_0''d_0''$. Thus the 0-level cone-axis annulus has a width of $D_0'd_0' = D_0d_0'''$ along a north (vertically up) radius through the central spot P_c, and a width $D_0d_0 = D_0''d_0''$ along a south radius. In short the annulus will be a trifle wider on the north radius, since the [b]-axis is outside of the precessing direction. Nevertheless one can find the center of the annulus along a north-south diameter through the central spot, and this gives the approximate location of b (the point where the b-axis cuts the film). Thus from film measurements one can readily get a value for the distance P_cb. The result obtained by this simplified method will be a trifle too large, and this error increases as the orientation gets worse. The approximate angular error of setting along the dial axis (e_D) can then be obtained since

$$\tan e_D = P_cb/s'. \tag{48}$$

Using this formula with the value of P_cb obtained from the film of Fig. 24*c* gave $e_D = 2°18'$, whereas the true value was 2°, an error of 15%.

If the setting is also off on a vertical axis, one may use the same method and formula to compute e_V, providing measurements for the location of b are made along an east-west diameter through the central spot P_c. The result obtained by this technique for the film of Fig. 24*e*, was 0°45′, which is too small by 25%. Since this last value is too small, whereas the above formula should lead to too large a result, it seems reasonable to suppose that any error inherent in the simplified formula is considerably less than the errors of measurement of the edges of the annulus.

Laue Streaks

Laue streaks (general radiation reflection trails) which appear on ordinary cone-axis films may be used for obtaining quite a precise orientation of a suitable single crystal, providing its symmetry is not

too low grade. Although most of the cone-axis photographs here reproduced were made with filtered radiation, enough polychromatic radiation was present to yield pronounced Laue streaks. As is well known any Laue streak represents the locus of Bragg reflections marked out by where a central row of the reciprocal lattice [that is, a line joining $n(hkl)^*$ points to $(000)^*$] cuts the sphere of reflection. In effect, as the radiation becomes of shorter wave length than that characteristic of the target metal, the translation values in the reciprocal lattice decrease. Just as any point on the reference band of a 0-level Weissenberg photo may be taken to represent $(000)^*$, and the Laue streaks on such a photo head towards this band, making an angle of 63°26′ with it if the instrument has an undistorted scale, so any point on the 0-ring of a cone-axis photo may be taken to represent $(000)^*$. This ring is characterized by a heavy circular Laue streak. In analogous fashion the 0-level line of a rotation photo may be marked by a pronounced Laue streak.

The easiest way to explain these Laue streaks on precession pictures seems to be in terms of movement of the levels of the reciprocal lattice. Thus in Fig. 14 as the wave length of the x-rays varies, the position of the 0-level plane R_0R_0' remains constant, but the spacing d^* between this and the adjacent parallel plane varies directly; that is, with shorter wave length get smaller d^*, and vice versa. Thus with shorter wave length points R_1 and R_1' move along the surface of the sphere of reflection towards R_0 and R_0' respectively. Note also that under these conditions a $\bar{1}$-level (regarding R_1R_1' as the $+1$-level) moves in close enough to R_0R_0' so that it will eventually cut the sphere of reflection; see Fig. 26. For any given wave length there is a symmetrical relationship between these two 1-levels across the 0-level. Thus the general radiation reflection trails often trace out paths from an n-level ring spot $x(hkn)^*$ across the 0-level ring [at a "spot" corresponding to $(000)^*$] towards some $\bar{n}$-level ring spot $x(hk\bar{n})$.*

Such streaks may be seen tracing out conic sections through spots on the n-rings. Thus in Fig. 20*b* the $n(1\bar{1}\bar{2})^*$ elliptical streak, shown as a dotted line in the upper left part of Fig. 20*a*, quite pronouncedly goes through the two $(1\bar{1}\bar{2})^*$ spots on the $\bar{1}$-ring and cuts across the 0-ring [at points which can be regarded as $(000)^*$ spots] heading towards the $(11\bar{2})^*$ spots of the 1-ring. The latter ring does not appear in the photo. Also pronounced is the $n(1\bar{1}0)^*$ Laue streak in Fig. 20*b* which appears near the top of Fig. 20*a* as the elliptical dash-dot line. On the original film of Fig. 20*b* this streak clearly goes through a pair of spots on the $\bar{2}$-ring whose indices should be $(2\bar{2}0)^*$. The corresponding $(\bar{1}\bar{1}0)^*$ streak shown near the base of Fig. 20*b* does not quite reach the $\bar{1}$-ring of the film, but it does cut the two $(\bar{2}\bar{2}0)^*$ spots.

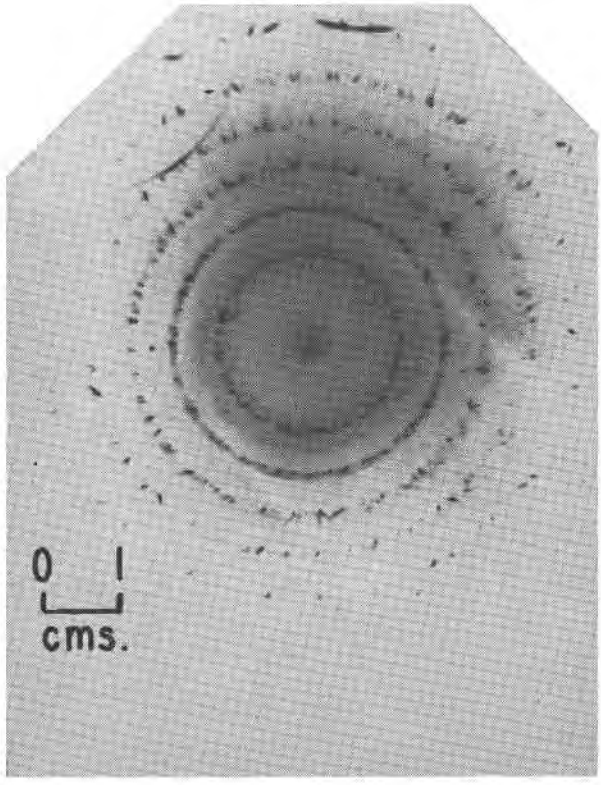

FIG. 26. Chalcanthite cone-axis photo. Same data as Fig. 24*a* except $\bar{\mu}=30°$. As usual the 0-ring is marked by a circular Laue streak. Inside it the $\bar{1}$-ring shows up very well; the central spot is hidden by Laue streaks associated with the $\bar{2}$-ring. Except for these, the most pronounced streaks on the original film are those just inside the $\bar{1}$-ring associated with spots on this ring.

As the wave length decreases, although the position of the 0-level (R_0R_0' of Fig. 14) remains constant, the translation units of the reciprocal net of this level (and of all others, too) also become smaller. Thus for non-characteristic radiation as the smaller-mesh 0-level grid shears through the sphere of reflection during precession, new directions of Bragg reflection are obtained along the 0-level cone of diffraction. This explains the pronounced circular Laue streak marking the 0-level cone-axis ring.

Of course the position of the 0-level R_0R_0' of Fig. 14 can be changed by altering the $\bar{\mu}$-angle; with decreasing angle R_0' moves along the sphere towards R_0. This yields a 0-level cone-axis ring which is smaller; moreover it also has fewer characteristic radiation diffraction spots on it,

since a smaller part of the 0-level grid then precesses through the sphere of reflection.

Figure 27 shows a series of cone-axis photos, all of which were made exactly like that of Fig. 20 except for the $\bar{\mu}$-angle. The Laue photo of Fig. 27*d* may be regarded as a special case of a cone-axis photo where $\bar{\mu}=0°$. Some of the zone-ellipses and spot-indices of this are indicated by the tracing of it shown as Fig. 27*f*. Here the major axes of the [011] ellipses mark $[c]^t$, and of the [110] ellipses is $[a]^t$. Also $[c^*]$ is tangent to [100] through *b*, and $[a^*]$ is tangent to [001] through *b*. Figure 27*e* is a print showing the combination of Figs. 27*c* & *d*. It will be noted that each spot of *d* lies near the inner focal point (the one closer to the center of the figure) of a Laue streak ellipse of *c*. If *d* (or better a trace-o-film copy of *f*) is similarly superposed on *a* or *b*, the same is found to be true. Thus it is fitting that the general radiation reflection trails of *a*, *b*, & *c* be called Laue streaks. Indeed the spots of Fig. 27*d* become in the cone-axis photos Laue streaks which are elliptical with major-axes[10] of lengths equivalent to $2\bar{\mu}$. The 1- and 2-rings are indicated on these cone-axis photos, and it is easily seen that many elliptical Laue streaks cut these without giving rise to spots. Of course only those streaks belonging to a Bragg reflecting plane of the proper level can yield spots on any given cone-axis ring.

TABLE 10. INDICES OF CONE-AXIS SPOTS, Fig. 27*b* & *c*

Cone-axis spot		Quadrant			
		NW	SW	SE	NE
b	1-ring	—	$\bar{1}\bar{1}\bar{1}$ & $2\bar{1}0$	$2\bar{1}1$ & $\bar{1}\bar{1}2$	$0\bar{1}2$ & $1\bar{1}1$
	2-ring	$22\bar{1}$	$\bar{2}2\bar{1}$	$\bar{2}\bar{2}2$	$1\bar{2}2$ & $2\bar{2}0$
c	1-ring	—	$\bar{1}\bar{1}\bar{1}$	$2\bar{1}1$	$1\bar{1}1$
	2-ring	$22\bar{1}$	$\bar{2}2\bar{1}$	$\bar{2}\bar{2}2$	$2\bar{2}0$

The indices of the spots (and associated Laue streaks) on the 1-ring (these are in circlets in Fig. 27*f*) and the 2-ring (these are in small squares in Fig. 27*f*) of the cone-axis photos of Fig. 27*b* & *c* are given in Table 10 (proceeding anticlockwise from the north position). The Laue streaks of Fig. 20*b* (the corresponding spots in Fig. 27*f* are in small triangles) are similarly indexed in Fig. 20*a*. It will be noted that Laue spots $(\bar{2}\bar{2}2)$ and

[10] The major axis as well as the minor axis of each Laue streak ellipse is equivalent to $2\bar{\mu}$; the corresponding Laue spot is not at a focal point, but is a distance equivalent to $\bar{\mu}$ from each vertex.

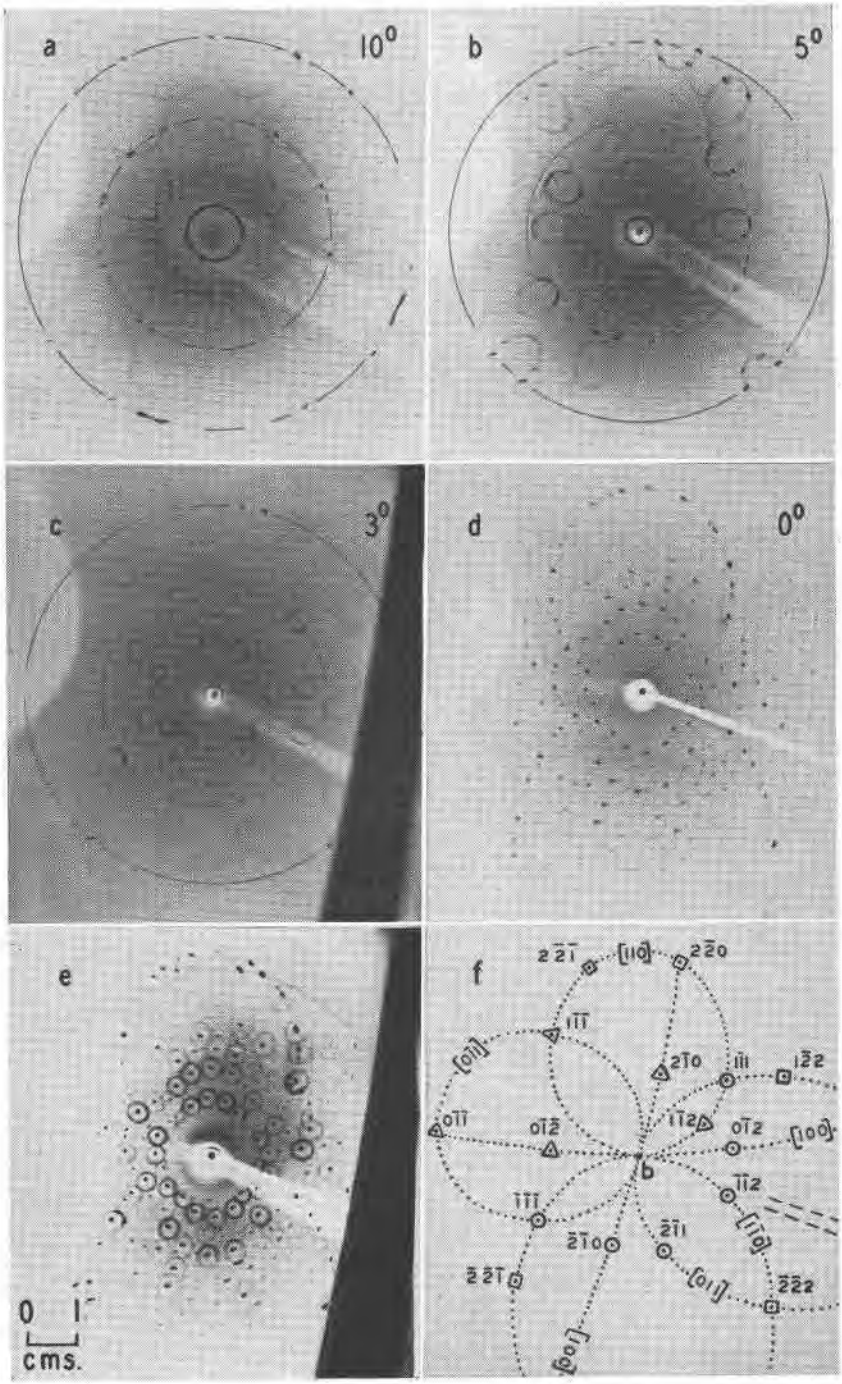

FIG. 27. Cone-axis and Laue photos of chalcanthite. Same data as Fig. 20 (except for $\bar{\mu}$ angles, which are given; also *b* and *d* were taken with *unfiltered* iron radiation). (*e*) is a composite print of *c* and *d*; (*f*) shows some of the spot and zone-ellipse indices of *d*.

($2\bar{2}0$) in Fig. 27*f* are given multiple indices. This is because they show up to have these values in Fig. 27*b* & *c* [though ($\bar{1}\bar{1}1$) and ($1\bar{1}0$) are present in Fig. 20]. It is obvious that the Laue streaks on a given cone-axis photo may be considered as representing the sum total of Laue photos which could be obtained by individual exposures from a non-moving crystal at each position of the $\bar{\mu}$-arc during a 360° precession.

In short the Laue streaks mark out conic sections on a cone-axis film. The axis of this general radiation cone (if the crystal is properly oriented) is normal to the film for the 0-ring spots, but is inclined in the case of *n*-level ring spots. If that generatrix of the general radiation cone which is most nearly parallel to the film is actually parallel to the film, the path traced is a parabola; if that generatrix is less inclined than this, the result is an ellipse; if more inclined, an hyperbola.

If a cone axis photo has well-developed Laue streaks cutting the 1-ring, it should be an easy matter to derive the reciprocal lattice net from it, and thus the spots could be indexed. For example one could take a suitably enlarged trace-o-film copy of the $\bar{1}$-ring of Fig. 20*b* and using each of the two spots on any one Laue streak as centers, draw circles of radius r_G (see Figs. 15 & 18) and find their points of intersection. One of these would mark a reciprocal lattice point. Given enough of these the grid could be prepared; some of the points of such a grid are shown in Fig. 20*a*. Thus from two cone-axis photos (one like Fig. 20*b*, another similar but with precession along [*a*]) one could derive all the geometrical constants of a triclinic unit cell (and the space group of a cell of higher symmetry), though one would hardly expect the results to be highly accurate.

Because of the low symmetry of chalcanthite the Laue streaks are not of help in orienting the crystal. In the case of sphalerite (Fig. 17*b*) however, certain trails are of great value in this connection. In particular the streaks which appear inside the 0-ring outlining a sort of lozenge (these show up very well on the original film) serve to give a very delicate check on the orientation, since the distances of these trails from the central spot vary quite perceptibly with but a tiny change in angular relations between the lattice planes and the direct beam. Similar trails of value in checking accurate orientation appear in the cone-axis photos of Fig. 28. Here in (*a*) the portions of the four streaks cutting the 1-ring which show up well inside this ring are of this character (the one at the lower left has been touched up a bit; it is perfectly clear on the original film). In (*b*) there are several valuable streaks inside the 0-ring; also the streaks along the horizontal (dial) axis inside the 2-ring. In (*c*) valuable streaks appear inside the 0-ring and also nearly tangent to the 1-ring in the NE & SW quadrants and cutting the 2-ring in the NW & SE quadrants.

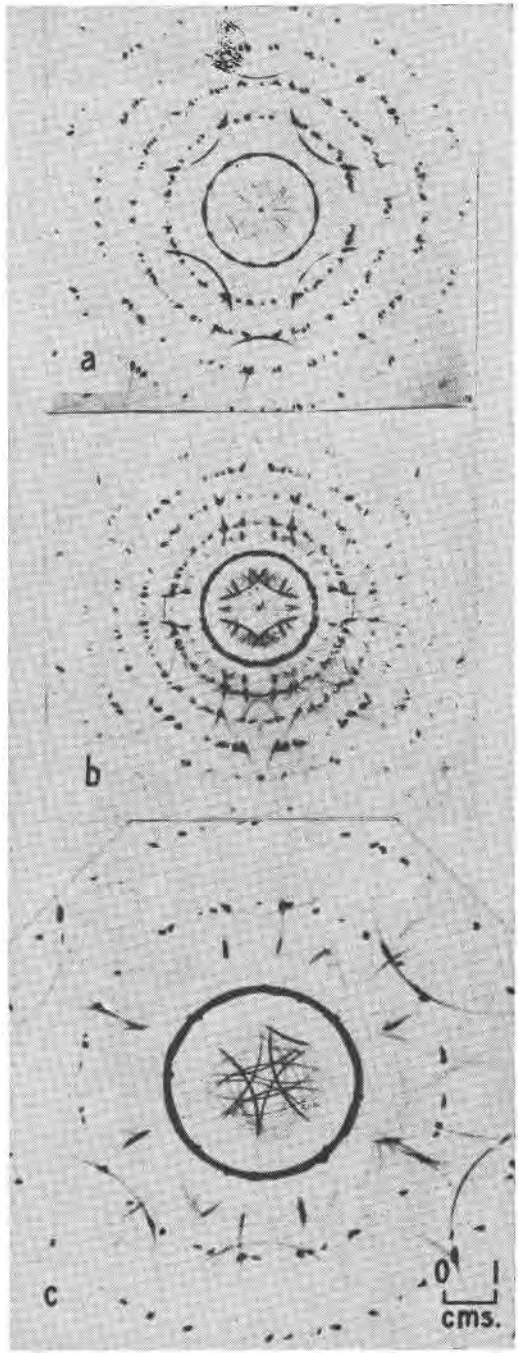

FIG. 28. Cone-axis pictures with $\bar{\mu}=20°$. (*a*) Quartz (hexagonal), precessing axis $(P)=[a^*]$, $D=[c]$, MoK$_\alpha$ radiation, $s'=30.22$ mm. (*b*) Natrophilite (orthorhombic, 0.60 :1:0.47) Branchville, Conn. $P=[b]$, $D=[c]$, MoK$_\alpha$, $s'=29.4$. (*c*) Adularia (monoclinic) Butte, Mont. $P=[b]$, $D=[a]$, CuK$_\alpha$, $s'=50.0$.

ACKNOWLEDGEMENTS: W. F. Schmidt did the photography (other than the *x*-ray work), and F. A. Johnson and F. L. Koucky helped with the drawings.

REFERENCES

BUERGER, M. J. (1944), The photography of the reciprocal lattice: *Amer. Soc. X-ray & Electron Diffraction* (now *American Crystallographic Association*), *Monogr.*, No. **1**, 37 pp.

FISHER, D. J. (1952*a*), Triclinic gnomonostereograms: *Am. Mineral.*, **37**, 83–94.

——— (1952*b*), The lattice constants of synthetic chalcanthite, etc., *Ibid.*, **37**, 95–114.

——— (1952*c*), Triclinic calculations, *Ibid.*, **37**, 697–699.

——— (1952*d*), *X*-ray precession techniques, *Ibid.*, **37**, 1036–1054.

Manuscript received July 23, 1952.